



Large-scale fabrication of structurally coloured cellulose nanocrystal films and effect pigments

Benjamin E. Droguet¹, Hsin-Ling Liang^{2,3}, Bruno Frka-Petesic¹, Richard M. Parker¹,
Michael F. L. De Volder², Jeremy J. Baumberg³ and Silvia Vignolini¹ ✉

Cellulose nanocrystals are renewable plant-based colloidal particles capable of forming photonic films by solvent-evaporation-driven self-assembly. So far, the cellulose nanocrystal self-assembly process has been studied only at a small scale, neglecting the limitations and challenges posed by the continuous deposition processes that are required to exploit this sustainable material in an industrial context. Here, we addressed these limitations by using roll-to-roll deposition to produce large-area photonic films, which required optimization of the formulation of the cellulose nanocrystal suspension and the deposition and drying conditions. Furthermore, we showed how metre-long structurally coloured films can be processed into effect pigments and glitters that are dispersible, even in water-based formulations. These promising effect pigments are an industrially relevant cellulose-based alternative to current products that are either micro-polluting (for example, non-biodegradable microplastic glitters) or based on carcinogenic, unsustainable or unethically sourced compounds (for example, titania or mica).

More-sustainable approaches to produce effect pigments and functional nanomaterials are being intensively searched for to replace inorganic and synthetic polymer components^{1–6}. In this context, the self-assembly of cellulose nanocrystals (CNCs) into structurally coloured films has attracted considerable interest in the scientific community and beyond as a potential candidate to produce more sustainable photonic pigments^{1,7,8}. However, while the understanding of the critical processes regulating the nanoscale self-assembly of CNCs has improved sufficiently to enable a wide range of optical applications^{9–12}, and with several companies now supplying nanocellulose in large volumes^{13,14}, the lack of scalable methodologies to produce large-area coloured CNC films remains the bottleneck for their commercial exploitation¹⁵. The deposition of CNC suspensions using a roll-to-roll (R2R) approach can produce transparent films^{16,17}; however, such techniques have so far failed to yield films with the cholesteric ordering required to produce structural colouration. The latter has been demonstrated only over relatively small areas, usually cast within shallow Petri dishes^{18–20}. Working with small-scale batches does not allow the challenges associated with large-scale production to be identified and addressed. For instance, continuous manufacturing processes, such as slot-die R2R, impose restrictions on the rheological properties of the deposited viscoelastic material. It needs to be sufficiently viscous to provide good coverage and to avoid dewetting and shrinkage of the coating upon drying, while still being able to self-assemble within the limited time window available for complete solvent evaporation during continuous processing. Meeting such requirements is challenging for aqueous CNC suspensions, as long evaporation times are typically required to allow for the self-assembly into vibrantly coloured CNC films^{21,22}. Furthermore, excessive shear (such as that obtained via blade casting) can easily disrupt any pre-existing cholesteric ordering^{23,24}.

In this work, we overcome these challenges and demonstrate an industrially relevant route to scale up the production of structurally

coloured films by casting a commercially available CNC suspension on a commercial R2R coating unit. Through optimization of the coating parameters affecting the self-assembly process, we fabricate metre-scale structurally coloured films with tuneable colour across the entire visible spectrum. Finally, we show that these structurally coloured R2R-cast films can be processed into vivid, water-stable photonic CNC microparticles that can be used as a sustainable effect pigment or ‘glitter’ for a wide variety of applications.

Large-area photonic CNC films and particles were produced using a pilot-scale R2R coating unit, whereby an aqueous CNC suspension was deposited and subsequently dried on top of a moving polymer substrate (the ‘web’), before being delaminated for further off-line processing into structurally coloured cellulosic microparticles. This process can be divided into several key steps, as summarized in Fig. 1a and described in detail in the Methods. First, corona discharge was performed in the central part of the web to activate the surface (Fig. 1b). This increases the surface energy of the hydrophobic polyethylene terephthalate (PET) web, which facilitates the subsequent wetting of the low-viscosity aqueous CNC suspension (Supplementary Fig. 1). This also allows for the pinning of the suspension, confining it within the hydrophilic–hydrophobic boundaries of the web and preventing uncontrolled flow of the suspension outside the deposition area. Deposition of the CNC suspension was then achieved by translating the web past an in-line slot-die, allowing for continuous, controlled coating (Fig. 1c). After deposition, the coated web was either dried statically under ambient conditions (Fig. 1d) or passed through a heating chamber (hot air dryer) across the R2R pathway to shorten the drying time (Fig. 1k). The latter enables a stepwise continuous deposition process to be achieved (Fig. 1e), as described in detail later. Examples of red, green and blue CNC films on a black PET web, as obtained from static drying under ambient conditions, are shown in Fig. 1g. Additionally, the resulting metre-scale CNC films can be peeled from the web using a blade to obtain free-standing films (Fig. 1f), as exemplified in Fig. 1h.

¹Bio-inspired Photonics Group, Yusuf Hamied Department of Chemistry, University of Cambridge, Cambridge, United Kingdom. ²Nanomanufacturing Group, Department of Engineering, University of Cambridge, Cambridge, United Kingdom. ³Nanophotonics Centre, Cavendish Laboratory, University of Cambridge, Cambridge, United Kingdom. ✉e-mail: sv319@cam.ac.uk

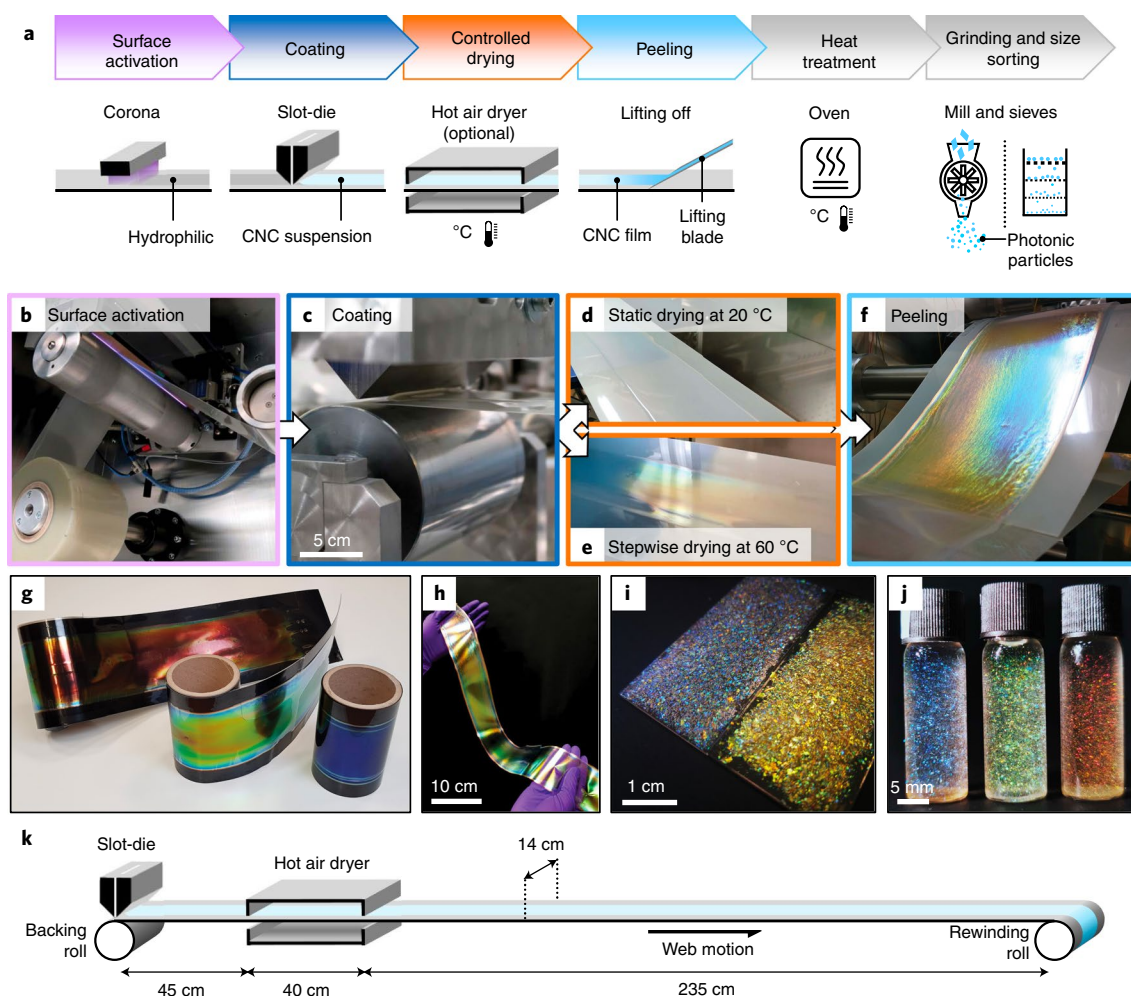


Fig. 1 | Overview of the R2R processing of a CNC suspension into photonic films and microparticles. **a**, Flow chart describing the key steps to prepare photonic CNC particles. **b**, Photograph of the corona etching step conducted after unwinding the web. **c**, Photograph of the slot-die depositing the CNC suspension onto the central region of the PET web. **d**, Photograph of a CNC suspension on the R2R web drying statically at room temperature. **e**, Photograph of a near-dry CNC film on the R2R web after passing through an in-line hot air dryer, with the web moving in a stepwise continuous manner. **f**, In-line peeling of a thick CNC film from the PET web. **g**, Red, green and blue R2R-cast CNC films deposited onto a black PET web. **h**, Free-standing R2R-cast CNC film. **i**, Pristine (left) and heat-treated (right) photonic CNC particles embedded in transparent varnish (prior to size sorting). **j**, Heat-treated photonic CNC particles that can be used as effect pigments, after size sorting and immersion, from left to right, in ethanol, 50% aqueous ethanol and water. **k**, Schematic of the R2R pathway, showing the position of the hot air dryer relative to the slot-die and the available length for static drying ($l_{R2R} = 3.2$ m). For reference, in **b-g** the width of the web is 14 cm.

Such CNC films can be subjected to thermal treatment, grinding and size sorting to produce structurally coloured particles that can find application as glitter (Fig. 1i) or effect pigments (Fig. 1j).

Optimization of casting conditions on a laboratory-scale coater

As the key slot-die deposition parameters for the quality of the final R2R films can be similarly controlled at smaller scales, their optimization was first performed on a laboratory-scale blade-coater. Notably, neither slot-die nor blade-cast deposition has been used so far to produce structurally coloured CNC films. For both deposition methods, the key parameters that should affect the optical appearance of the resultant CNC films are the coating gap, g_c , and the coating speed, v_c . To investigate their impact, we first optimized the deposition of the CNC suspension on the blade-coater (Methods). Independently adjusting g_c and v_c leads to variable thicknesses and shear rates during deposition, which can affect the initial ordering of the cholesteric structures and impact the kinetics

of the self-assembly upon drying. To decouple these two effects, we investigated the effect of g_c and v_c at a fixed shear rate $\dot{\gamma} = v_c/g_c$. The quality of the optical response was then assessed by considering the intensity of the reflected peak position and its width, as they depend on the alignment and periodicity of the cholesteric structure and the thickness of the film²⁵.

As shown in Fig. 2a, blade-cast films with a macroscopically uniform blue appearance were produced in all cases from the same CNC suspension (6 wt%, sonicated for 2.24 s ml⁻¹) with a constant shear rate $\dot{\gamma} = 2.2$ s⁻¹. As expected, a larger coating gap (here with a higher coating speed) leads to a greater film thickness (reaching a maximal thickness of 14 μm for $g_c \geq 900$ μm and $v_c \geq 2.0$ mm s⁻¹). Importantly, as shown in Fig. 2b,c, the films cast with $g_c = 700$ μm and $v_c = 1.5$ mm s⁻¹ reached the maximum achievable reflectance with a thickness of only 10.5 μm (additional optical analysis with right-circularly polarized (RCP) spectra is reported in Supplementary Fig. 2a). This implies that the cholesteric structures of the films produced with this technique are relatively well aligned

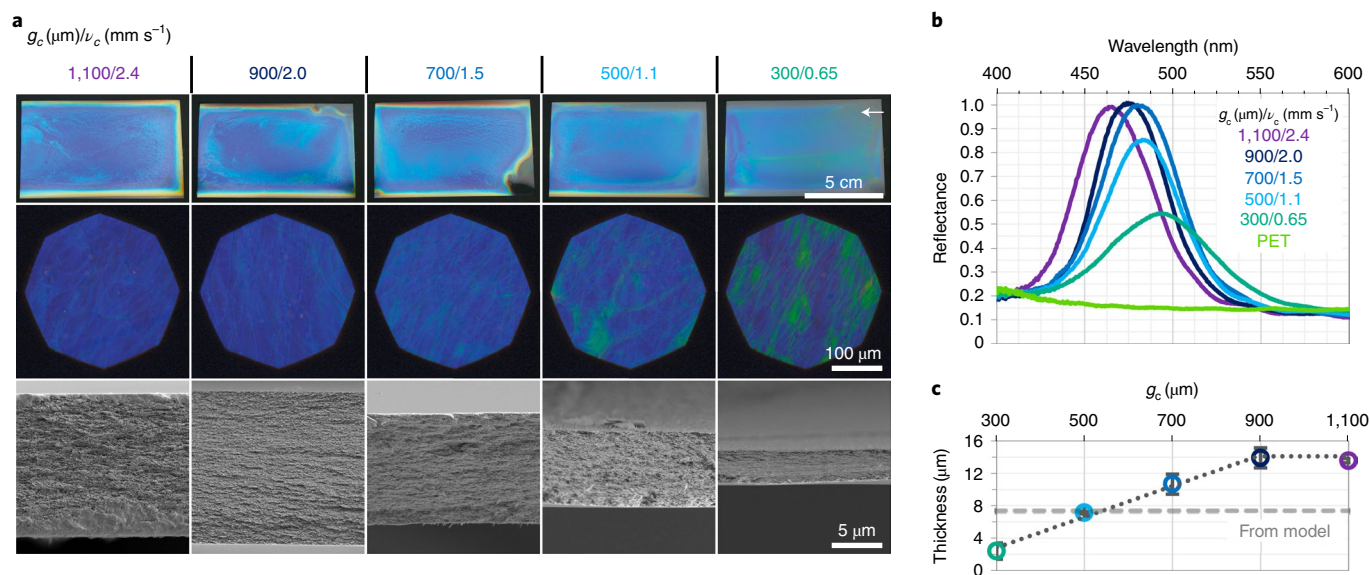


Fig. 2 | Film thickness and optical properties versus coating parameters. **a**, Photographs (row 1), left-circularly polarized (LCP) optical micrographs (row 2) and SEM cross-sections (row 3) of the blade-cast films, prepared from a CNC suspension sonicated for 2.24 s ml⁻¹ and deposited at $\dot{\gamma} = 2.2$ s⁻¹. The arrow indicates the direction of the blade motion. **b**, Corresponding LCP reflectance spectra of the films in **a**, averaged over 15+ positions. **c**, Thickness of the films versus the coating gap. The dashed grey line highlights the theoretical minimum thickness required for a CNC film to reach maximal reflectance. The points correspond to the mean average film thickness, recorded across $N = 4$ –9 positions, with the error bars corresponding to the standard deviation.

(Fig. 2c)^{23,26}, as, for ideal cholesteric films, the theoretical thickness required to achieve maximal reflectivity is ~ 8 μm (calculated from both numerical²⁷ and analytical²⁸ models and taking CNC refractive indices as $n_e = 1.590$ for the extraordinary index, defined parallel to the alignment direction of CNCs (that is, the local nematic director), and $n_o = 1.514$ for the ordinary index, defined perpendicular to it (ref. 11), see Supplementary Fig. 3). Coating the suspension using a larger gap resulted only in a small blueshift (Fig. 2b), as the larger volume of deposited suspension resulted in a longer drying time, as previously reported²⁵. Below $g_c = 700$ μm and $v_c = 1.5$ mm s⁻¹, the blue films also exhibit green patches visible on the microscope, leading to a less intense and broader reflectance peak. As the shear rate was kept constant for all films, we do not expect this decrease in reflection to arise from a transient disruption of the cholesteric order during the deposition. However, a reduced thickness is associated with a faster evaporation time, which decreases the time permitted for self-assembly and affects the quality of the resulting cholesteric order. Such observations are in good agreement with previous observations on CNC self-assembly: a shorter time triggers a kinetic trapping of the cholesteric domains before they manage to coalesce into the homogeneous structure needed to produce a uniform optical response²⁵. From these observations, casting parameters of $g_c = 700$ μm and $v_c = 1.5$ mm s⁻¹ led to satisfactory films and were used henceforth.

Blue, green and red blade-cast CNC films were prepared by applying increasing tip-sonication treatment to the same initial CNC suspension (Fig. 3a), as previously reported for dish-cast films^{29–31}. As an additional control, films cast in Petri dishes from the same suspensions showed similar spectra (Supplementary Figs. 4 and 2b), confirming that scaling up or down the deposition conditions does not noticeably impact the optical quality. Note that all samples reported here were sonicated directly at 6 wt% CNC concentration, for which the suspension is in a biphasic state (Supplementary Fig. 5). As also observed for thin dish-cast films, increasing the total sonication energy delivered to the suspension results in a widening of the peak, along with a decrease of the maximum reflectivity, the latter being particularly pronounced for the longest sonication treatment

(Fig. 3b). Finally, the incorporation of macromolecular additives, such as hydroxypropyl cellulose (HPC), has been reported to redshift the reflected colour of a CNC film while also suppressing edge inhomogeneities and acting as a plasticizer³². To this end, we fabricated CNC–HPC composite films, as reported in Supplementary Fig. 6. We found that inclusion of 40 wt% HPC imparted a strong redshift to the blade-coated CNC film but also increased disorder at the microscopic level. More importantly in the context of this work, it resulted in a less brittle film with greater adherence to the PET substrate, which also made delamination more difficult.

Large-scale coating using a R2R process

To increase productivity, most industrial R2R casting processes utilize methods to increase the evaporation rate of the employed solvent, for instance by increasing the temperature using additional furnaces or with hot airflows downstream of the coating stage. To understand how elevated temperature affects the self-assembly process, the deposited suspensions were placed on a hotplate at 60 °C and both the drying time and the optical quality of the final films were monitored. In this condition, coloured films were produced in about 20 min (versus 5.5 h at room temperature; Fig. 3a). When compared to drying in ambient conditions, this dramatically faster evaporation rate induced inhomogeneities of colour in the films, with a reflectance peak that was about 30% weaker (Fig. 3b) and slightly redshifted (Supplementary Fig. 7). These observations can be explained by the presence of a stronger convective flow of the suspension at higher temperature and a shorter time for the CNCs to self-organize and self-assemble prior to kinetic arrest. However, these effects can be partially compensated by the deposition thickness or the CNC formulation (via ionic strength or sonication treatment) to meet the desired trade-off between commercially viable production rates and final yield in terms of CNC consumption per surface area.

The optimization of the initial CNC formulation and the calibration of the deposition conditions were then translated to a pilot-scale R2R system, enabling the production of flexible, metre-scale CNC coatings with uniform red, green and blue structural colouration

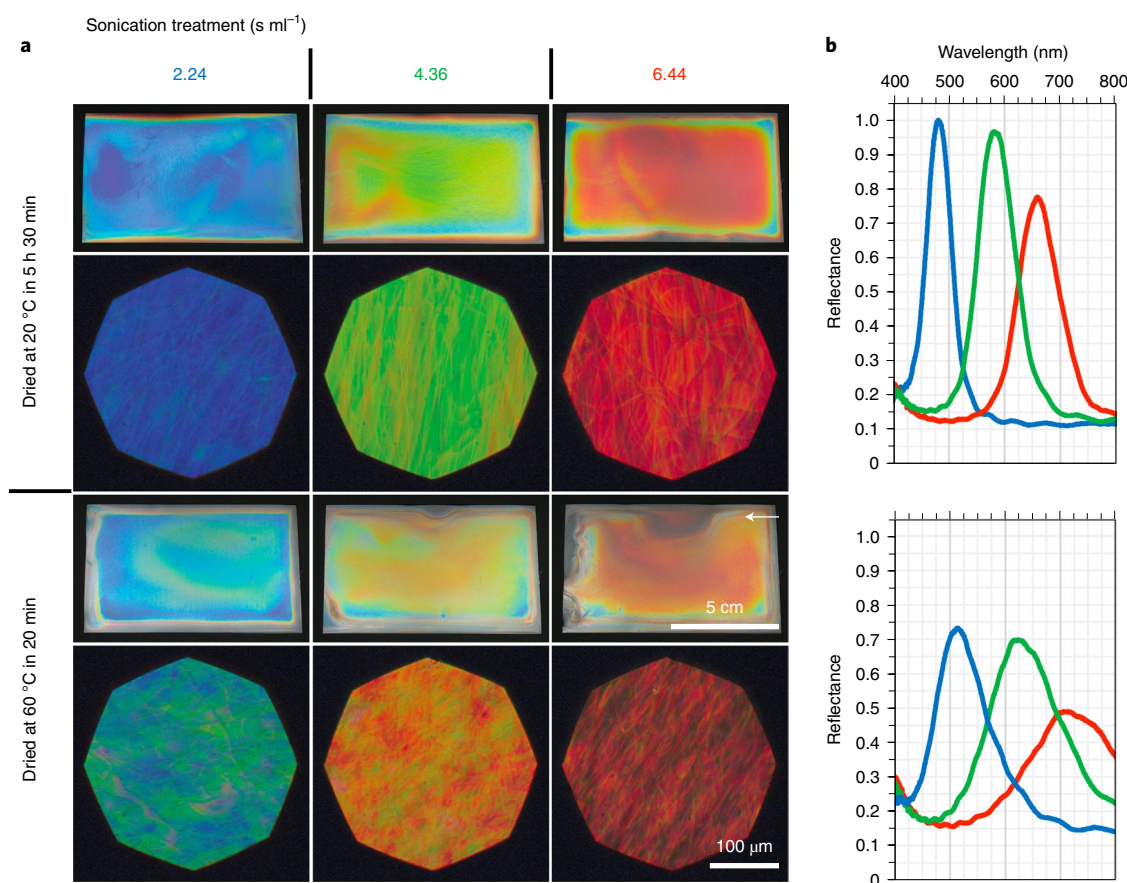


Fig. 3 | Effect of sonication and drying conditions on the visual appearance of blade-cast CNC films. a, Macroscopic photographs and LCP optical micrographs of CNC films prepared from suspensions sonicated for 2.24 (left), 4.36 (middle) and 6.44 s ml^{-1} (right), and dried either at 20 °C (top) or 60 °C (bottom). For all films $g_c = 700 \mu\text{m}$ and $v_c = 1.5 \text{ mm s}^{-1}$. The arrow indicates the direction of the blade motion. **b,** Corresponding LCP reflectance spectra of samples dried at room temperature (top) and on a hotplate (bottom), averaged over 15+ locations.

(Fig. 1f). To produce these films, the deposited CNC suspension was held at rest during the evaporative drying process. This compromise arises from the combination of the web pathway length ($l_{\text{R2R}} = 3.2 \text{ m}$) and the minimum continuous translational speed of the equipment used ($v_c = 0.1 \text{ m min}^{-1} \approx 1.67 \text{ mm s}^{-1}$), not allowing sufficient time for the film to fully dry before the coated web reaches the rewinding roll (time, $t = l_{\text{R2R}}/v_c \approx 30 \text{ min}$). To overcome this engineering limitation and demonstrate the continuous production of photonic CNC films, the R2R process was modified to include an in-line hot air dryer (to accelerate evaporation) and stepwise translation (to reduce the effective deposition speed of the web), as described in Fig. 1k. In contrast to ‘static drying’, this ‘stepwise continuous’ process allows for the limitation of the finite length of the web pathway to be overcome, while maintaining good optical quality (Fig. 4). In industrial R2R coaters, these drying-time issues are typically addressed by having more drying units in series.

Two stepwise deposition methods were used, denoted ‘coarse’ and ‘fine’ steps (Supplementary Fig. 8 and Methods), with both processes having the same effective translation speed ($v_{\text{eff}} \approx 0.2 \text{ mm s}^{-1}$), resulting in each section of the coated web spending a total of 30 minutes passing through the hot air dryer. Using the coarse steps as an example, the CNC suspension was found to be sufficiently dried upon exiting the hot air dryer (temperature, $T = 60 \text{ °C}$) such that it already exhibited structural colour (Supplementary Video 3 and Supplementary Fig. 9). Complete evaporation was then achieved under ambient conditions prior to reaching the end of the R2R pathway, resulting in a photonic film with good

optical quality (Supplementary Fig. 10 and Supplementary Table 1). Notably, this method enables the production of films that span beyond the limit of the web pathway of our machine (Fig. 4a; $l_{\text{film}} = 4.2 \text{ m} > l_{\text{R2R}} = 3.2 \text{ m}$), validating that the process of photonic CNC film fabrication can be decoupled from the physical limits of the R2R machine (Supplementary Fig. 11).

By utilizing fine steps, the translation of the web was approximated to an uninterrupted deposition at a lower effective speed (Supplementary Fig. 8), overcoming the limitation of the minimum translation speed on our R2R machine. Importantly, this fine-step, stop-start coating method did not result in notable discontinuities of the resultant film. By varying the temperature of the hot air dryer from 20 °C to 60 °C, the interplay between accelerated drying and the optical properties of the resultant CNC film could be assessed. As shown in Fig. 4b, all conditions produced vibrant blue films with good optical alignment, consistent with the absence of reflection of RCP light. Shortening the drying time by increasing the temperature resulted in a small redshift combined with a weakened optical response (Fig. 4c), as previously noted for the blade-cast analogues (Fig. 3). However, allowing for the differences in thickness (Supplementary Table 2), the stepwise films have comparable reflectance to the film dried statically. As a result, we can conclude that films produced using the fine-step process at 60 °C maintain a good optical appearance while drying sufficiently fast as to enable continuous and uninterrupted fabrication.

Importantly, the relative flexibility of the PET substrate enables straightforward delamination of the R2R-cast CNC films (Fig. 1f)

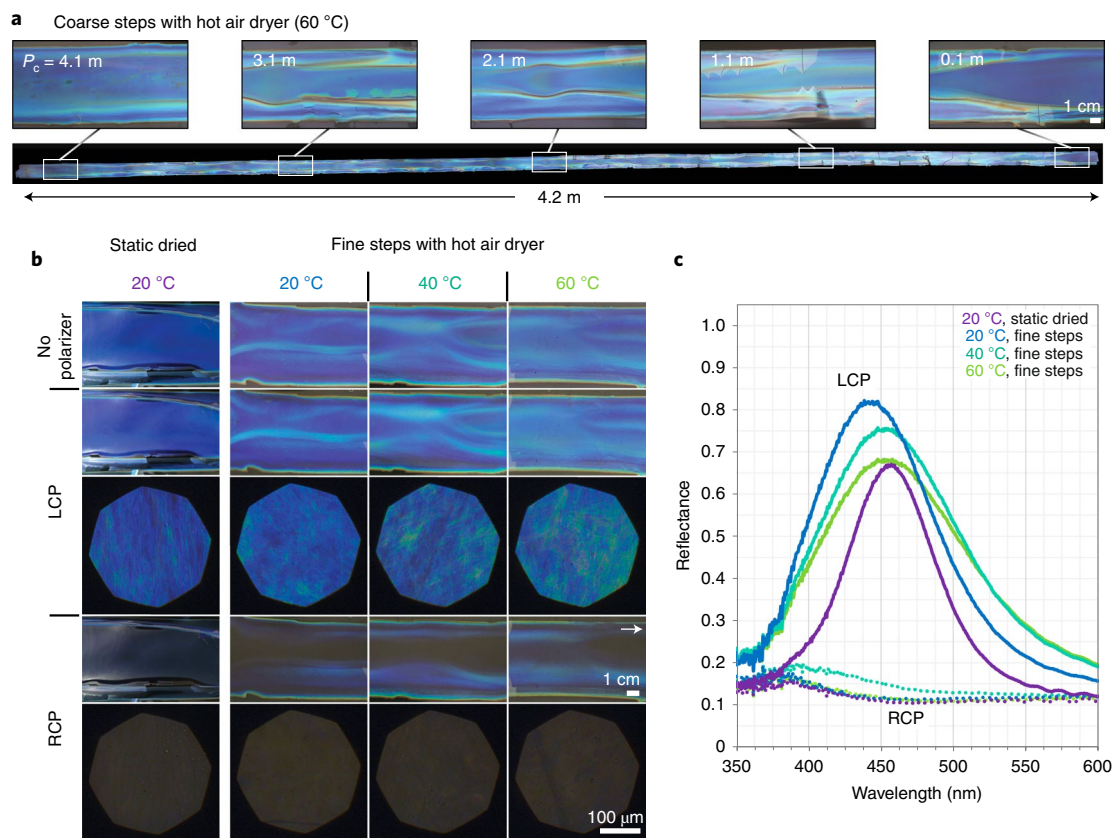


Fig. 4 | Optical properties of CNC films cast by R2R and dried either statically or with stepwise continuous translation through an in-line hot air dryer. **a**, Images of a 4.2-m-long blue R2R-cast film with insets showing the optical appearance at different positions (P_c) along the length. Here the position is defined relative to the beginning of the deposition. **b**, Photographs (rows 1, 2 and 4) and optical micrographs (rows 3 and 5) of R2R-cast CNC films (sonicated for 2.24 s ml^{-1}) recorded through LCP and RCP filters. The arrow indicates the direction of the web motion. **c**, Corresponding LCP and RCP reflectance spectra of the free-standing films reported in **b**. The LCP reflectance spectra are averaged over 80+ positions along the film.

to obtain free-standing films (Fig. 1b). For thicknesses of $14 \mu\text{m}$ and more, in-line peeling could be achieved by placing a blade between the web and the CNC film (Supplementary Video 4), which was then transferred onto a second substrate for additional off-line processing, as described later. For smaller thicknesses, films can still be detached, but due to their fragility, substantial cracking occurs.

Preparation of water-stable photonic microparticles

Finally, the industrial relevance of this scalable R2R approach is illustrated by further processing the free-standing films into structurally coloured microparticles that can be used as effect pigments and glitter. This addresses the current limitations, in terms of both the yield and the colour criteria needed, for such particles to be commercialized, unlike previous attempts that used non-scalable dish casting and reported poor optical performance³³. This processing was achieved by sequentially employing heat treatment, grinding and size sorting (Supplementary Fig. 12a,b) to yield flake-like particles with average diameters in the range of tens to hundreds of micrometres (Fig. 5). The optical response of the largest particles obtained is comparable to the progenitor R2R-cast film, whereas the smallest particles, while remaining visibly coloured to the naked eye, present weaker reflection peaks (Fig. 5b and Supplementary Fig. 13). In the bright-field optical microscopy images, some of the smaller particles appear dark and less coloured; however, the same particles observed in dark-field images reveal strong colour (Supplementary Fig. 14). This indicates that the main cause of the apparent lack of reflection in bright-field images is primarily due to

a larger variation in the orientation of the particles with respect to the viewing direction.

Applying a heat treatment (30 min at 180°C) to the R2R-cast films before grinding plays a key role. First, it prevents the degradation of the surfaces of the film during the grinding step. Scanning electron microscopy (SEM) observations revealed that the cholesteric structure is not damaged by the grinding (Fig. 5d) and that the particle surface remains smooth with distinct facets and sharp edges (Fig. 5c). This suggests that the grinding process probably breaks distinct cholesteric domains at their defect boundaries rather than indiscriminately fracturing the films³⁴. Second, the heat treatment makes the microparticles much more stable, as they do not redisperse after immersion in various solvents, including water. Unlike in a previous report³³, the improved resistance of their cholesteric structure to both mechanical and chemical processing remains effective even after several months (samples kept immersed in water for more than a year and a half are still intact and colourful; Supplementary Fig. 12d). Furthermore, Fourier transform infrared spectroscopy and thermogravimetric analysis suggest little degradation of the nanocrystals for heat treatment temperatures below 220°C (Supplementary Fig. 15c,d).

The improved mechanical and solvent resistance of the heat-treated films prepared from pH-neutralized CNCs (Na-CNCs) can be explained by partial desulfation and the release of tightly bound water from their surface, allowing for stronger attractive interactions between individual CNCs³⁵ as well as the presence of sodium ions³⁶. The resulting stability to water immersion is remarkable

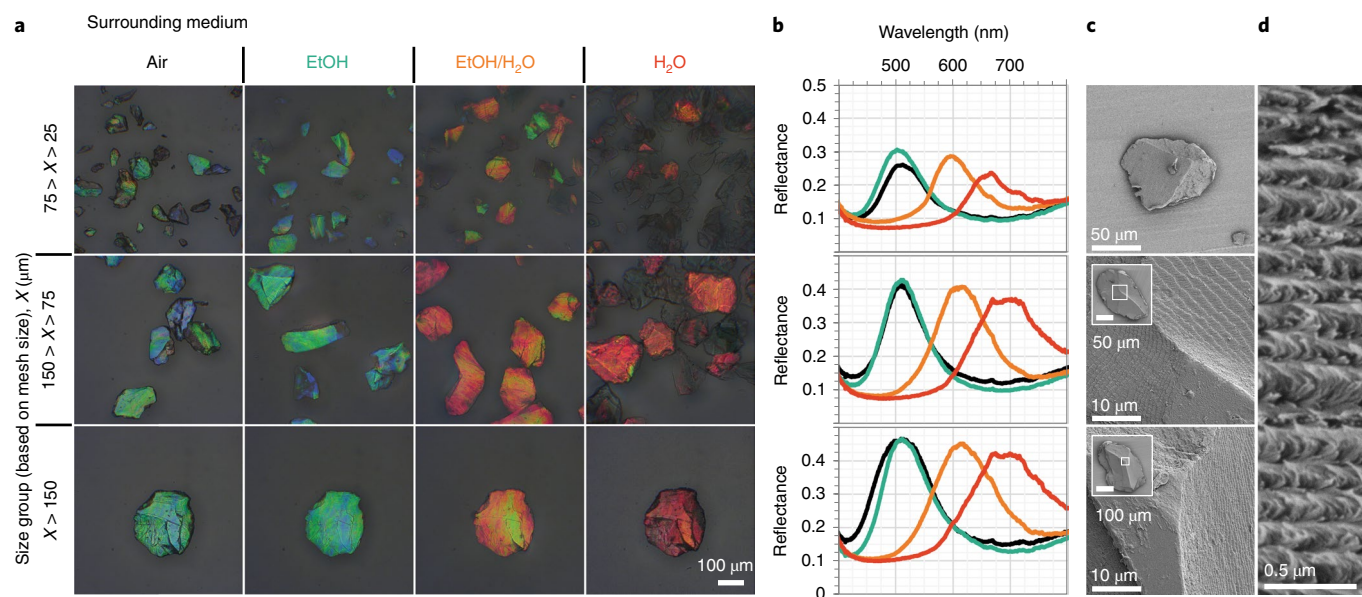


Fig. 5 | Photonic CNC microparticles. **a**, Micrographs of size-sorted and heat-treated photonic CNC microparticles prepared from a green R2R-cast film (sonicated for 4.36 s ml^{-1}), as observed in air (column 1), in pure ethanol (column 2), in a 50:50 (by weight) water/ethanol mixture (column 3) and in pure water (column 4). Microscopic views for the largest size depict the same particle. **b**, Corresponding total reflectance spectra of the size-sorted particles in the same four media, averaged over 10+ locations. **c**, SEM top views exemplifying photonic CNC particle morphology after grinding for each size group. **d**, SEM cross-section of a CNC particle showing the typical Bouligand arches, characteristic of the CNC cholesteric order.

given that Na-CNCs are otherwise known to individually redisperse much better than acidic CNCs (H-CNCs) after a freeze- or spray-drying step^{33,37}. The use of Na-CNCs also reduces blackening of the film after heat treatment³⁸, which is otherwise observed in films made from H-CNC suspensions^{33,39,40}. Instead, the heat treatment gives only a slight golden tint to the films, improving the contrast of the reflected colour (Supplementary Fig. 15a,b). Substantial blackening is however visible at the very edge of CNC films (Supplementary Fig. 16d), where the films are thicker due to weak ‘coffee ring’ effects^{41,42}, but this impacts only a small fraction of the film and can also be decreased by scaling up on a wider web⁴³.

The compatibility of the photonic CNC particles with various solvent mixtures is summarized in Fig. 5a. Green CNC particles, made from grinding a green R2R-cast film, did not visibly change colour after immersion in ethanol compared to in air, as confirmed by the reflection spectra reported in Fig. 5b. These observations indicate that there is no significant swelling in ethanol. By contrast, immersion of the particles in either a 1:1 (mass ratio) mixture of ethanol and water or in pure water led to a red-shift of respectively 100 nm and 175 nm, consistent with a gradual swelling with the increasing polarity of the solvent (Fig. 5a,b and Supplementary Fig. 12c). The slight decrease in peak reflectivity is consistent with the decrease of the overall birefringence Δn of the films upon solvent uptake. The degree of swelling is stable over time, which is an essential requirement when adjusting the colour of the particles for their subsequent use in a given formulation (for example, in the presence of ions, surfactants or solvents), as illustrated in Supplementary Fig. 12c–f. This swelling is also reversible: the original colour of the particles in the dried state was retrieved upon solvent evaporation, suggesting no partial dispersion of the CNCs (Supplementary Fig. 17 and Supplementary Video 5). Finally, the flake-like nature of the particles and their angular-dependent response allows for a characteristic metallic effect⁴⁴: by controlling the orientation of these particles, the macroscopic angular response can be tailored. As an example, particles dispersed in liquid have a strong angular-dependent colouration and a glittery appearance

(Supplementary Video 6), while the same or even smaller particles added into a coating display a much more uniform appearance (Supplementary Figs. 14, 18 and 19). The visual quality of our photonic CNC microparticles is validated by comparing them against commercial alternatives employed in comparable proportion and in the same coating geometry (Supplementary Fig. 19).

Conclusions

In summary, we optimized the self-assembly of CNC suspensions into photonic films using a continuous R2R coating technique. This allowed for the fabrication of metre-scale structurally coloured CNC films with an excellent optical response. Furthermore, we showed that grinding the obtained films after a further heat treatment yields particles that can be used as effect pigments and glitter. Importantly, these particles retained their optical response after a year without fading or redispersing, even in water. This work demonstrates that a self-assembled bio-sourced nanomaterial can be successfully combined with a high-throughput technique (such as R2R casting), leading to the fabrication of large-scale, structurally coloured cellulosic films. We expect the industrial relevance of this process, as conceptualized in Supplementary Fig. 21, will spark interest in the commercial development of eco-friendly photonic pigments to replace non-biodegradable microplastic glitters and unsustainable or unethically produced inorganic effect pigments in paints, inks, cosmetics, beverages, labelling and packaging.

Online content

Any methods, additional references, Nature Research reporting summaries, source data, extended data, supplementary information, acknowledgements, peer review information; details of author contributions and competing interests; and statements of data and code availability are available at <https://doi.org/10.1038/s41563-021-01135-8>.

Received: 13 November 2020; Accepted: 17 September 2021;
Published online: 11 November 2021

References

- Green, D. S., Jefferson, M., Boots, B. & Stone, L. All that glitters is litter? Ecological impacts of conventional versus biodegradable glitter in a freshwater habitat. *J. Hazard. Mater.* **402**, 124070 (2021).
- Pfaff, G. & Reynnders, P. Angle-dependent optical effects deriving from submicron structures of films and pigments. *Chem. Rev.* **99**, 1963–1981 (1999).
- European Commission. *Environmental and Health Risks of Microplastic Pollution* (European Union Publications, 2019). <https://doi.org/10.2777/54199>
- ten Kate, A., Schipper, L., Kiezebrink, V. & Remmers, M. *Beauty and a Beast: Child Labour in India for Sparkling Cars and Cosmetics* (Centre for Research on Multinational Corporations, 2016).
- Proposal for Harmonised Classification and Labelling: Titanium Dioxide CLH Report* (French Agency for Food, Environmental and Occupational Health & Safety, 2008).
- Younes, M. et al. Safety assessment of titanium dioxide (E171) as a food additive. *Eur. Food Saf. Auth. J.* **19**, e06585 (2021).
- Frka-Petescic, B. & Vignolini, S. So much more than paper. *Nat. Photon.* **13**, 365–367 (2019).
- Klockars, K. W. et al. Asymmetrical coffee rings from cellulose nanocrystals and prospects in art and design. *Cellulose* **26**, 491–506 (2019).
- Lagerwall, J. P. F. et al. Cellulose nanocrystal-based materials: from liquid crystal self-assembly and glass formation to multifunctional thin films. *NPG Asia Mater.* **6**, e80 (2014).
- Zhang, Y. P., Chodavarapu, V. P., Kirk, A. G. & Andrews, M. P. Nanocrystalline cellulose for covert optical encryption. *J. Nanophoton.* **6**, 063516 (2012).
- Zhao, T. H. et al. Printing of responsive photonic cellulose nanocrystal microfilm arrays. *Adv. Funct. Mater.* **29**, 1804531 (2019).
- Giese, M., Blusch, L. K., Khan, M. K., Hamad, W. Y. & MacLachlan, M. J. Responsive mesoporous photonic cellulose films by supramolecular cotemplating. *Angew. Chem. Int. Ed.* **53**, 8880–8884 (2014).
- Reid, M. S., Villalobos, M. & Cranston, E. D. Benchmarking cellulose nanocrystals: from the laboratory to industrial production. *Langmuir* **33**, 1583–1598 (2017).
- Reiner, R. S. & Rudie, A. W. in *Production and Applications of Cellulose Nanomaterials* (eds Postek, M. T. et al.) 21–24 (TAPPI Press, 2013).
- Vanderfleet, O. M. & Cranston, E. D. Production routes to tailor the performance of cellulose nanocrystals. *Nat. Rev. Mater.* **6**, 124–144 (2021).
- Chowdhury, R. A., Clarkson, C. & Youngblood, J. Continuous roll-to-roll fabrication of transparent cellulose nanocrystal (CNC) coatings with controlled anisotropy. *Cellulose* **25**, 1769–1781 (2018).
- Koppolu, R. et al. Continuous roll-to-roll coating of cellulose nanocrystals onto paperboard. *Cellulose* **25**, 6055–6069 (2018).
- Parker, R. M. et al. Hierarchical self-assembly of cellulose nanocrystals in a confined geometry. *ACS Nano* **10**, 8443–8449 (2016).
- Gray, D. G. Recent advances in chiral nematic structure and iridescent color of cellulose nanocrystal films. *Nanomaterials* **6**, 213 (2016).
- Revol, J.-F., Godbout, L. & Gray, D. G. Solid self-assembled films of cellulose with chiral nematic order and optically variable properties. *J. Pulp Pap. Sci.* **24**, 146–149 (1998).
- Gicquel, E., Bras, J., Rey, C. & Jean, B. Impact of sonication on the rheological and colloidal properties of highly concentrated cellulose nanocrystal suspensions. *Cellulose* **7**, 7619–7634 (2019).
- Shafiei-Sabet, S., Hamad, W. Y. & Hatzikiriakos, S. G. Rheology of nanocrystalline cellulose aqueous suspensions. *Langmuir* **28**, 17124–17133 (2012).
- Haywood, A. D. & Davis, V. A. Effects of liquid crystalline and shear alignment on the optical properties of cellulose nanocrystal films. *Cellulose* **24**, 705–716 (2017).
- Diaz, J. A., Wu, X., Martini, A., Youngblood, J. P. & Moon, R. J. Thermal expansion of self-organized and shear-oriented cellulose nanocrystal films. *Biomacromolecules* **14**, 2900–2908 (2013).
- Parker, R. M. et al. The self-assembly of cellulose nanocrystals: hierarchical design of visual appearance. *Adv. Mater.* **30**, 1704477 (2018).
- Zhu, B. et al. Hyperspectral imaging of photonic cellulose and implications for self-assembly pathways. *ACS Nano* **14**, 15361–15373 (2020).
- Berreman, D. W. Optics in stratified and anisotropic media: 4×4-matrix formulation. *J. Opt. Soc. Am.* **62**, 502–510 (1972).
- de Vries, H. Rotatory power and other optical properties of certain liquid crystals. *Acta Crystallogr.* **4**, 219–226 (1951).
- Beck, S., Bouchard, J. & Berry, R. Controlling the reflection wavelength of iridescent solid films of nanocrystalline cellulose. *Biomacromolecules* **12**, 167–172 (2011).
- Dong, X. M., Revol, J.-F. & Gray, D. G. Effect of microcrystallite preparation conditions on the formation of colloid crystals of cellulose. *Cellulose* **5**, 19–32 (1998).
- Foster, E. J. et al. Current characterization methods for cellulose nanomaterials. *Chem. Soc. Rev.* **47**, 2609–2679 (2018).
- Walters, C. M., Boott, C. E., Nguyen, T. D., Hamad, W. Y. & MacLachlan, M. J. Iridescent cellulose nanocrystal films modified with hydroxypropyl cellulose. *Biomacromolecules* **21**, 1295–1302 (2020).
- Bardet, R., Roussel, F., Coindeau, S., Belgacem, N. & Bras, J. Engineered pigments based on iridescent cellulose nanocrystal films. *Carbohydr. Polym.* **122**, 367–375 (2015).
- Wang, P. X., Hamad, W. Y. & MacLachlan, M. J. Structure and transformation of tactoids in cellulose nanocrystal suspensions. *Nat. Commun.* **7**, 11515 (2016).
- Beck, S. & Bouchard, J. Auto-catalyzed acidic desulfation of cellulose nanocrystals. *Nord. Pulp Pap. Res. J.* **29**, 6–14 (2014).
- Lin, N. & Dufresne, A. Surface chemistry, morphological analysis and properties of cellulose nanocrystals with gradiented sulfation degrees. *Nanoscale* **6**, 5384–5393 (2014).
- Dong, X. M. & Gray, D. G. Effect of counterions on ordered phase formation in suspensions of charged rodlike cellulose crystallites. *Langmuir* **13**, 2404–2409 (1997).
- Chauve, G., Mauran, D., Fraschini, C. & Bouchard, J. Critical discussion on the thermal behavior of sulfated cellulose nanocrystals. *TAPPI J.* **15**, 383–391 (2016).
- D’Acerno, F., Hamad, W. Y., Michal, C. A. & MacLachlan, M. J. Thermal degradation of cellulose filaments and nanocrystals. *Biomacromolecules* **21**, 3374–3386 (2020).
- D’Acerno, F., Ohashi, R., Hamad, W. Y., Michal, C. A. & MacLachlan, M. J. Thermal annealing of iridescent cellulose nanocrystal films. *Carbohydr. Polym.* **272**, 118468 (2021).
- Gençer, A., Van Rie, J., Lombardo, S., Kang, K. & Thielemans, W. Effect of gelation on the colloidal deposition of cellulose nanocrystal films. *Biomacromolecules* **19**, 3233–3243 (2018).
- Mu, X. & Gray, D. G. Droplets of cellulose nanocrystal suspensions on drying give iridescent 3-D “coffee-stain” rings. *Cellulose* **22**, 1103–1107 (2015).
- Dufresne, A. *Nanocellulose: from Nature to High Performance Tailored Materials* (De Gruyter, 2012). <https://doi.org/10.1515/9783110254600>
- Frka-Petescic, B., Kamita, G., Guidetti, G. & Vignolini, S. Angular optical response of cellulose nanocrystal films explained by the distortion of the arrested suspension upon drying. *Phys. Rev. Mater.* **3**, 045601 (2019).

Publisher’s note Springer Nature remains neutral with regard to jurisdictional claims in published maps and institutional affiliations.

© The Author(s), under exclusive licence to Springer Nature Limited 2021

Methods

CNC suspension preparation. An aqueous CNC suspension was purchased from the University of Maine Process Development Center (batch no. 2015-FPL-077, [CNC] = 11.8 wt%, pH-neutralized form, 1.2 wt% sulfur content). The suspension was diluted with ultrapure water to 6 wt% in 50 ml tubes (Corning Falcon with conical bottom) and sonicated in an ice bath using an ultrasonic disintegrator (Fisherbrand 505 Sonic Dismembrator 500 W, amplitude = 40%, tip diameter = 12.7 mm).

Suspensions for laboratory-scale blade-cast CNC films were prepared by batches of 25 ml and sonicated for 56, 109 and 161 s to produce respectively blue, green and red films upon casting. Suspensions for large-scale R2R deposition were prepared by batches of 45 ml, in which case the sonication time was respectively scaled up to 101, 196 and 290 s. This allows for the energy delivered per volume of CNC suspension by the tip sonicator to be kept constant and corresponds to treatments of 2.24, 4.36 and 6.44 s ml⁻¹. After equilibrating the suspension for 1–3 days, the denser anisotropic phase was separated and collected for further use^{45,46}. In the case of the HPC–CNC composite presented in Supplementary Fig. 6, the sample was prepared as before from a CNC suspension sonicated for 2.24 s ml⁻¹, in which HPC (Nisso, SSL grade, nominal molecular weight = 40 kDa) at a concentration of 40 wt% with respect to the dry CNC mass was added prior to casting.

Substrate preparation. PET was used as a substrate for CNC film deposition (HIFI Film PMX727 in the ‘laboratory scale’ blade-casting set-up and Mitsubishi Polyester Film, Hostaphan RN 500 as the web on the R2R set-up), with the surface selectively activated to control wetting. For the laboratory-scale set-up, the PET sheets (thickness = 125 μm, length = 120 mm, width = 80 mm) were secured to the coating stage and a plasma etcher was used for surface activation (Emitech K1050X plasma etcher, vacuumed air atmosphere, 50 W, 5 min). By contrast, R2R deposition required the use of a reel (web thickness = 500 μm, web width = 140 mm), and corona discharge (Corona Supplies, 0.3 kW) was used to activate the continuously moving substrate (speed = 0.1 m min⁻¹ ≈ 1.67 mm s⁻¹). This larger thickness was required on the R2R to inhibit any stress-induced web warping^{47,48}, which can lead to unwanted suspension flow during drying (Supplementary Videos 1 and 2). Note that the PET was manually masked with tape in both configurations but could easily be continuously applied and removed, as proposed in Supplementary Fig. 21, or a fixed mask could be utilized.

Deposition of photonic CNC castings. Laboratory-scale blade-cast CNC films were prepared using a bespoke blade-coater with a maximum casting length of ~30 cm (Supplementary Fig. 22). This coater is composed of a motor (Reliance Cool Motion Stage) that can move a flat stage along a track, above which a coating applicator (BEVS 1806/A50) was mounted at a fixed position. To prepare a CNC film, the PET substrate was attached to the stage on three sides, with the trailing edge free to allow excess CNC suspension to be removed. The blade was set to the desired height above the substrate and the coating applicator positioned near the front of the rectangular PET sheet. The CNC suspension (~3.5 ml) was deposited in front of the blade and the stage moved at the selected speed such that an area of 6 × 10 cm was uniformly coated.

Large-scale deposition of the CNC suspension was achieved using a modified R2R casting system (Coatema Coating Machinery, Smartcoater 28) equipped with a custom-made slot-die (casting width = 10 cm, internal reservoir = 22 ml). The slot-die was made of two screw-joined aluminium plates separated by a 125-μm-thick spacer shim configured with a slot opening of 100 mm and positioned perpendicular to the web. A syringe pump (New Era) was used to continuously dispense the CNC suspension to the slot-die, with the dispensing rate (~6 ml min⁻¹) adjusted depending on the desired film thickness and coverage width. The distance between the slot lips and the substrate was controlled with a thickness feeler gauge. Web holders were placed so that the average distance between each support was 30 cm. The substrate was levelled before casting using a bullseye spirit air bubble level (Thorlabs LVL01) at several positions along the web path and at the middle of the width. Shear rates were calculated from the translational speed and the coating gap thickness.

For ‘static drying’, the web was translated through the R2R system at the lowest accessible speed ($v_c = 0.1 \text{ m min}^{-1} \approx 1.67 \text{ mm s}^{-1}$), with a maximum casting length of ~3.2 m, corresponding to the limits of the web pathway. The web translation was then stopped, and the deposited suspension was allowed to dry under ambient conditions. Alternatively, to investigate faster drying, a blown-air heating chamber (length ≈ 40 cm, $T = 20\text{--}60^\circ\text{C}$) was placed across the R2R pathway after the coating step (as shown in Fig. 1k). This allowed for a continuous stepwise deposition and drying process, whereby the translation of the web was divided into multiple steps interrupted by stationary rest periods. Two step sizes were demonstrated (denoted ‘coarse’ and ‘fine’) as plotted in Supplementary Fig. 8: for the coarse process, the web was translated at $v_c = 1.67 \text{ mm s}^{-1}$ in steps of 20 cm every 15 min, while for the fine process, the web was translated at the same speed, but in steps of 5 cm every 3.75 min. In both cases, this corresponds to an effective translation speed of $v_{\text{eff}} \approx 0.2 \text{ mm s}^{-1}$.

Drying conditions. The CNC suspension was dried at ambient conditions for the dish-cast films and the laboratory-scale blade-cast films. Drying was typically complete within a few hours, depending on the amount of material deposited and the surface area. Additionally, laboratory blade-coated films were also dried more

rapidly using a hotplate set at 60 °C. Despite using the lowest speed accessible on the R2R machine ($v_c = 0.1 \text{ m min}^{-1}$), the time required for the drying of a large-scale CNC suspension at ambient conditions exceeded the available length of our pilot-scale R2R machine. As such, either (1) drying was performed without motion over several hours until film formation and is denoted as ‘static dried’, or (2) the deposited CNC suspension was slowly translated through an in-line hot air dryer ($T = 20\text{--}60^\circ\text{C}$) using the ‘stepwise continuous’ translation process described above, allowing for the drying process to be accelerated such that the film was dry before reaching the end of the web pathway.

Photonic CNC particle preparation and size sorting. The R2R-cast CNC film was detached from the substrate web by placing a thin PET blade (attached to an upper collection web) at an angle to the substrate web. The CNC was initially manually peeled over a few centimetres and then completed by translating the substrate web at a constant speed (as depicted in Fig. 1a and shown in Supplementary Fig. 12a and Supplementary Video 4). The CNC film was subsequently broken down into centimetre-long pieces and heat-treated in a laboratory muffle furnace (Nabertherm, P330) set at 180 °C for 30 min. The CNC film was finally ground using a rotary blade (Cookworks electric coffee grinder PCML-2012, 150 W). The photonic CNC particles were sequentially size sorted using three sieves with decreasing mesh sizes of 150, 75 and 25 μm (Endecotts). The median size of the particles for each size category was retrieved from SEM images by highlighting the contours of individual particles and fitting with the Ferret area function in ImageJ (Supplementary Fig. 23).

Optical microscopy and imaging. Polarized optical microscopy (Zeiss AxioScope A1) images of the CNC films were taken using a ×20 objective (Zeiss EC Epiplan Apochromat, numerical aperture = 0.3), whereas images of the photonic CNC particles were taken with a ×10 objective (Zeiss EC Epiplan Apochromat, numerical aperture = 0.6), unless stated otherwise. The light reflected by the CNC films attached to the PET substrate passed through a quarter-wave plate and an orientable linearly polarizing filter, which together can filter either LCP or RCP light reflected by the sample. A beam-splitter allowed the light to be directed to a charge-coupled device camera (Thorlabs DCC3240C) and to a fibre-coupled spectrometer (Avantes AvaSpec HS2048), mounted in confocal configuration with the plane of the objective using a lens (Thorlabs AC254-050-A). Such a configuration allows for interrogating a defined region of the microscope field of view. A 600-μm-core optical fibre (Thorlabs FC-UV600-2-SR) was used for measuring the CNC films with the ×20 objective, whereas a 200-μm-core optical fibre (Thorlabs FC-UV200-2-SR) was used for the photonic CNC microparticles with the ×10 objective. As a result, spectra were acquired over ~100-μm-wide and ~66-μm-wide spots, respectively. Unless stated otherwise, all the spectra of CNC cast films were acquired attached to the PET web, rather than free-standing, and normalized to the reflection of a silver mirror (Thorlabs PF10-03-P01) in one polarization channel (LCP), such that a perfectly aligned cholesteric sample would reflect 100% intensity. Each reported spectrum is the average of several measurements (see as an example Supplementary Fig. 24 for individual spectra and their average).

Photographs and videos. Photographs of the CNC films on a black background and Supplementary Video 6 were taken using a 20 MP digital camera (Huawei P10) at a fixed working distance and illumination. A mask was placed around the laboratory scale film to hold it flat without covering the edges of the film. Other images were taken using a 40 MP digital camera (Huawei P30 Pro). Time-lapse videos of Supplementary Videos 1, 2 and 4 were recorded with a 12.2 MP digital camera (Apple iPhone SE 1st) while for Supplementary Video 3 a webcam (Logitech HD Pro C920) and a 40 MP digital camera (Huawei P30 Pro) were used. Supplementary Video 5 was performed using the microscope set-up described above.

Scanning electron microscopy. Images were taken using a Tescan MIRA3 FEG-SEM, operated in high vacuum mode at 4 kV accelerating voltage and at a working distance of 3–4 mm. Samples were mounted on aluminium stubs with conductive carbon tape, and sputter-coated using a palladium target (Emitech K550).

Angular-resolved optical spectroscopy. Measurements were carried out using a bespoke laboratory goniometer: a lamp (Thorlabs SLS201L/M) was used as the light source, and a spectrometer (AvaSpec-HS2048XL, Avantes) was used to analyse the scattered optical signal. The sample was mounted on a rotating stage in the centre of the goniometer and illuminated (via an optic fibre $\Phi = 1,000 \mu\text{m}$) with a collimated incident beam on the sample surface (light spot size $\Phi \approx 6 \text{ mm}$). A detector was mounted on an arm attached to a motorized rotation stage and coupled the scattered light into an optic fibre ($\Phi = 600 \mu\text{m}$) connected to the spectrometer. The recorded light intensity was normalized with respect to a white Lambertian diffuser (Labsphere USRS-99-010), while the exposure time was adjusted using an automated high dynamic range method⁴⁹. Measurements were recorded at a fixed incident light angle (taken as either 0° or 30°, defined from the normal of the sample interface), and by scanning the scattered spectral intensity collected with the rotating detector at various outgoing angles.

Rheology. Sweep rheological measurements were performed using a rotational rheometer (TA Instruments DHR-2) equipped with a 40 mm parallel Peltier steel

plate geometry, using a gap of approximately 900 μm and applying CNC suspension (1 ml) on a temperature-regulated stage (20 °C).

Fourier-transform infrared (FT-IR) spectroscopy. FT-IR spectroscopy was performed on pristine and a series of heat-treated R2R-cast CNC films directly placed over the window of the spectrometer (Perkin Elmer, Spectrum 400). Each spectrum results from 16 scans on one location of each sample. Curves were normalized to the peak at 2,889 cm^{-1} .

Thermogravimetric analysis (TGA). The measurement was collected on a thermo-balance (Mettler Toledo TGA/SDTA 851) with a heating rate of 2 °C min^{-1} , under a flow of nitrogen gas (80 ml min^{-1}).

Data availability

Additional data relating to this publication are available from the University of Cambridge data repository (<https://doi.org/10.17863/CAM.64239>).

References

45. Klockars, K. W. et al. Effect of anisotropy of cellulose nanocrystal suspensions on stratification, domain structure formation and structural colors. *Biomacromolecules* **19**, 2931–2943 (2018).
46. Honorato-Rios, C. et al. Fractionation of cellulose nanocrystals: enhancing liquid crystal ordering without promoting gelation. *NPG Asia Mater.* **10**, 455–465 (2018).
47. Tardy, B. L. et al. Tessellation of chiral-nematic cellulose nanocrystal films by microtemplating. *Adv. Funct. Mater.* **29**, 1808518 (2019).
48. Kamita, G. et al. Biocompatible and sustainable optical strain sensors for large-area applications. *Adv. Opt. Mater.* **4**, 1950–1954 (2016).

Acknowledgements

This work was supported by the Engineering and Physical Sciences Research Council (EP/R511675/1 for S.V.; EP/N016920/1 for H.-L.L., J.J.B., M.D.V. and S.V.), by the European Union's Horizon 2020 Marie Skłodowska-Curie research and innovation programme (H2020-MSCA-ITN-2016 722842 for B.E.D and S.V.) and the European Research Council (ERC-2014-STG H2020 639088 for B.F.-P., R.M.P. and S.V.; ERC-2017-POC 790518 for S.V.). We thank F. Firth for performing the thermogravimetric analysis characterization.

Author contributions

The concept of R2R-manufactured photonics was conceived by J.J.B., M.D.V. and S.V.; CNC suspensions, films and particles were prepared and characterized by B.E.D.; R2R experiments were realized by B.E.D. and H.-L.L.; B.F.-P. and R.M.P. provided critical feedback on results. The manuscript was written by B.E.D., R.M.P., B.F.-P. and S.V. with input from all authors.

Competing interests

The authors declare no competing interests.

Additional information

Supplementary information The online version contains supplementary material available at <https://doi.org/10.1038/s41563-021-01135-8>.

Correspondence and requests for materials should be addressed to Silvia Vignolini.

Peer review information *Nature Materials* thanks Jay Guo and the other, anonymous, reviewer(s) for their contribution to the peer review of this work.

Reprints and permissions information is available at www.nature.com/reprints.